ICJK

Journal of Geo-Energy and Environment
http://dx.doi.org/10.62762/JGEE.2026.780406

RESEARCH ARTICLE

Study on Reservoir Space Characteristics and Gas Storage Mechanism of Low-Rank Coal Reservoir in Junggar Basin

Yuqing Chen[1,*] **and Yi Wang**[1]

[1] Xinjiang Yaxin Coalbed Methane Resource Technology Research Co., Ltd., Urumqi 830011, China

Abstract

The Junggar Basin contains widely distributed Jurassic low-rank coal seams (Badaowan Fm. J_1b, Xishanyao Fm. J_2x) with abundant coalbed methane (CBM) resources. Integrating proximate analysis, maceral identification, vitrinite reflectance, low-temperature N_2 adsorption, high-pressure mercury intrusion, and NMR, this study characterizes the petrological properties, pore-space characteristics, and gas storage mechanisms of J_1b and J_2x low-rank coals in the Baijiahai–Dinan area. Results show: J_1b is bright coal (vitrinite: 74.1%–88.3%, R_o: 0.67%), while J_2x ranges from semibright to dull coal (vitrinite: 57.2%, R_o: 0.71%), corresponding to long-flame coal–lignite stage. J_2x coal exhibits better reservoir properties (porosity: 9.4%; permeability: 19.64 mD) with well-developed meso/macropores favorable for free-gas storage; J_1b coal has abundant micropores offering greater adsorption capacity. Low-temperature N_2 adsorption curves classify pores as Type A (cylindrical/slit-shaped), B (parallel-plate/wedge-shaped), and C (closed-end wedge-shaped), with J_2x showing more diverse pore types and higher meso/macropore proportions. A hierarchical adsorption model for low-rank coal was developed: micropores fill rapidly at low pressure, transition pores approach monolayer saturation, and meso/macropores remain in unsaturated monolayer adsorption. Critical desorption pressures are 3.7–4.7 MPa for J_2x and 4.5–6.8 MPa for J_1b. Free-gas storage is controlled by both microscopic pore competition and macroscopic geological conditions. This study provides a key reference for CBM exploration and development in the Baijiahai–Dinan area.

Keywords: junggar basin, low-rank coal, pore space, pore structure, gas storage mechanism, adsorbed gas, free gas.

1 Introduction

Coalbed methane (CBM) is an important unconventional natural gas resource, and its exploration and development are of great significance for alleviating the imbalance between natural gas supply and demand in China and ensuring energy security. Low-rank CBM resources account for approximately 43.5% of China's total CBM

Submitted: 11 May 2026
Revised: 04 August 2026
Accepted: 12 August 2026
Published: 02 September 2026

Vol. 3, **No.** 1, 2027.
10.62762/JGEE.2026.780406

***Corresponding author:**
✉ Yuqing Chen
3483415970@qq.com

Citation
Chen, Y., & Wang, Y. (2026). Study on Reservoir Space Characteristics and Gas Storage Mechanism of Low-Rank Coal Reservoir in Junggar Basin. *Journal of Geo-Energy and Environment*, 3(1), 1–15.

© 2026 by the Authors. Published by Institute of Central Computation and Knowledge. This is an open access article under the CC BY license (https://creativecommons.org/licenses/by/4.0/).

resources [1]. The Junggar Basin is a large Jurassic low-rank coal-bearing basin in western China. Its CBM resources at depths shallower than 2,000 m amount to 2.2×10^{12} m^3, ranking fourth in China [2]. In recent years, deep CBM tests in the Junggar Basin have yielded encouraging daily gas production of approximately 1×10^4 m^3, indicating considerable exploration potential [3, 4]. However, sedimentary and coal-evolution conditions vary greatly among different blocks of the Junggar Basin, resulting in marked differences in coal-reservoir properties. The intrinsic controlling factors of the reservoirs require further detailed analysis, which currently constrains the selection of CBM enrichment zones and optimization of reservoir-stimulation technologies [4, 5].

Coal reservoirs constitute a "dual-porosity" structural system composed of pores and fractures [6]. In low-rank coal, CBM occurs in both adsorbed and free states, and its storage and migration are closely related to the pore-fracture system of the coal reservoir [5]. The microscopic pore structure not only provides abundant adsorption sites for gas but also controls matrix permeability [6]. Qualitative and quantitative characterization of coal-reservoir pore-fracture systems directly affects the accurate determination of gas content and the formulation of development plans [7].

Numerous studies in China and elsewhere have investigated the pore structure of coal reservoirs and gas storage mechanisms. With respect to pore-characterization methods, low-temperature N_2 adsorption, mercury intrusion, nuclear magnetic resonance (NMR), and CT scanning have been widely used to characterize coal pore structures, but most studies have focused on individual experimental analyses rather than integrated multi-method characterization. Regarding gas storage mechanisms, the Langmuir monolayer adsorption theory is commonly used to analyze coal adsorption behavior; however, it is not applicable to low-rank coal [8–10]. Meanwhile, quantitative experimental studies of free-gas storage mechanisms in deep CBM remain lacking. Therefore, this study combines CO_2, N_2, high-pressure mercury intrusion, and multiple complementary methods for integrated characterization; develops an adsorption-theory model applicable to low-rank coal based on the adsorption process within individual pores; and systematically investigates free-gas storage mechanisms from microscopic to macroscopic scales, with the aim of providing a scientific basis for CBM exploration and development in the study area.

This study focuses on the low-rank coal reservoirs of the Lower Jurassic Badaowan Formation (J_1b) and Middle Jurassic Xishanyao Formation (J_2x) in the Baijiahai–Dinan area of the Junggar Basin. The geological setting, experimental methods, pore-structure characterization results, and gas storage mechanisms are presented and discussed in the following sections.

2 Geological Setting

The Junggar Basin, located in northern Xinjiang, is a large composite superimposed basin in western China. Its first-order tectonic units include the Western Uplift, Central Depression, Eastern Uplift, and Ulungur Depression [11, 12]. The Baijiahai–Dinan study area is located in the eastern Junggar Basin and tectonically lies at the eastern end of the Central Depression. It is bounded by the Kelameili Mountains to the north and by the Shaxi Fault, separating it from the Shazhang fault-fold belt, to the east [11, 14]. The tectonic framework of the Baijiahai–Wucaiwan area was largely established during the Hercynian period. Tectonic conditions remained stable during deposition of the Lower and Middle Jurassic strata, whereas the Yanshanian movement caused substantial uplift and erosion of the northeastern Baijiahai Uplift [13].

The principal coal-bearing strata in the study area are the Lower Jurassic Badaowan Formation (J_1b) and the Middle Jurassic Xishanyao Formation (J_2x) [3, 10]. The Badaowan Formation comprises fluvial–lacustrine coal-bearing deposits dominated by gray-green and gray sandstone and mudstone, with interbedded conglomerate and coal seams. It is 34.49–452.3 m thick and unconformably overlies Triassic or Carboniferous strata [11]. The Xishanyao Formation is a coal-bearing succession composed of gray to dark-gray mudstone, silty mudstone, argillaceous siltstone, sandstone, and coal seams. It is 70–390 m thick, generally 100–150 m, and thickens overall from north to south and from the basin margin toward the basin interior [10, 14].

During deposition of the Badaowan Formation, the eastern Junggar area was topographically higher in the northeast and lower in the southwest. Alluvial-fan systems developed along the piedmont of the Kelameili Mountains and graded southwestward into braided-river–meandering-river alluvial plains, with coal accumulating in local waterlogged depressions. During deposition of the Xishanyao Formation, three

to four coal seams, several to tens of meters thick, developed in the study area. Together with mudstone, siltstone, and sandstone, these seams formed multiple depositional cycles. Each cycle begins with sandstone or sandy mudstone, fines upward, and is capped by a coal seam [10, 14].

3 Samples and Experimental Methods

3.1 Sample Collection

The samples were collected from wells Mei 006 and Jia Tan 2 in the Baijiahai–Dinan area of the Junggar Basin. Four J_1b coal cores were collected from Well Mei 006, and six J_1b coal cores and five J_2x coal cores were collected from Well Jia Tan 2, for a total of 15 samples. Immediately after collection, the samples were sealed to preserve their original pore structures and fluid-occurrence states as much as possible.

3.2 Experimental methods

This study integrated multiple experimental techniques covering three categories: coal petrology and quality analysis, pore-structure characterization, and gas-storage performance evaluation.

3.2.1 Coal Petrology and quality analysis

Proximate analysis was conducted in accordance with Chinese standard GB/T 212–2008 to determine moisture, ash, volatile matter, and fixed carbon contents. True and apparent densities were measured using the pycnometer method. Maceral identification and vitrinite reflectance measurements were performed microscopically in accordance with GB/T 8899–2013 and GB/T 6948–2008. Ultimate analysis was performed using an elemental analyzer to determine C, H, N, and S contents. Mineral composition was analyzed by X-ray diffraction (XRD).

3.2.2 Pore-structure characterization

(1) Because the BJH method is unreliable for quantitatively characterizing micropores smaller than 2 nm, this study combined low-temperature N_2 adsorption with low-pressure carbon dioxide (CO_2) adsorption.

Low-temperature N_2 adsorption was conducted in accordance with GB/T 19587–2004 [15]. Nitrogen adsorption-desorption isotherms were measured volumetrically at 77 K; the specific surface area was calculated using the BET equation, and the BJH method was used to calculate the pore-size distribution of mesopores and some macropores. Micropores were characterized by low-pressure CO_2 adsorption, and their specific surface area and pore volume were accurately calculated using a density functional theory (DFT) model.

Gas-adsorption characterization of the coal microstructure essentially involves volumetric measurement of changes in gas adsorption under isothermal conditions at ultra-low temperature.

The principle of specific-surface-area measurement is to use gas molecules as probes with a known molecular cross-sectional area. Under specified conditions, the gas molecules cover the entire surface of the sample by adsorption, and the surface area is obtained by multiplying the number of adsorbed molecules by the molecular cross-sectional area. At low temperature (77 K), when the relative pressure p/p_0 is between 0.05 and 0.35, nitrogen adsorption on the solid surface approximately satisfies the assumptions of the multilayer BET theory, allowing the specific surface area to be calculated using the BET equation. When $p/p_0 < 0.05$, the adsorbed amount is too low and measurement errors can readily occur; when $p/p_0 > 0.05$, intermolecular interactions among adsorbed layers and capillary condensation cause large differences in adsorption energy between molecular layers, violating the assumption that the adsorption energies of all layers above the first are equal.

$$\frac{1}{W\left(\frac{P_0}{P}-1\right)} = \frac{1}{W_m C} + \frac{(C-1)}{W_m C}\left(\frac{P}{P_0}\right)$$

where W is the gas adsorption capacity at pressure P, W_m is the monolayer adsorption capacity, C is the BET constant, and P/P_0 is the relative pressure (the ratio of equilibrium pressure P to saturated vapor pressure P_0). After W_m is obtained, S_{BET} can be calculated using the following equation.

$$S_{BET} = N_m \times \delta = \frac{W_m N_d}{M}$$

where N_m is the number of molecules in the monolayer, δ is the cross-sectional area of an adsorbate molecule, N_d is Avogadro's constant, and M is the molar mass of the gas.

The pore-size distribution is calculated by the BJH method using the Kelvin equation.

$$\ln\left(\frac{P}{P_0}\right) = -\left(\frac{2\gamma v \cos\theta}{r_k RT}\right)$$

where γ is the surface tension of the condensed liquid, v is the molar volume of the adsorbate condensed on the material surface, θ is the contact angle between the condensed surface and the pore wall, and r_k is the radius of curvature of the condensed surface. When nitrogen is used as the adsorbate, the Kelvin equation can be rewritten as follows:

$$r_k = \frac{4.15}{\log \frac{P_0}{P}}$$

The sum of the adsorbed-layer thickness t and r_k gives the pore radius. When $p/p_0 > 0.3$, condensation begins, and t and r_k can be calculated separately.

(2) High-pressure mercury intrusion was conducted in accordance with GB/T 21650.1–2008. The maximum mercury-intrusion pressure was 200 MPa, corresponding to a lower pore-size limit of approximately 7.2 nm. Mercury intrusion porosimetry has been demonstrated to be an effective method for characterizing the mesopore and macropore systems of low-rank coal reservoirs in the Junggar Basin [16].

Mercury-intrusion measurement is based on the concept proposed by Washburn, whereby an external force drives non-wetting liquid mercury into pores, and the work required to create the wetted area is equal to the work required to force mercury into cylindrical pores. The following equation can therefore be established:

$$p\pi r^2 l = -2\pi r l \sigma \cos\theta$$

After rearrangement, the classical Washburn equation is obtained as follows:

$$D = 2r = \frac{4\sigma \cos\theta}{P}$$

where D and r are the pore diameter and radius of the coal, respectively; θ is the mercury–coal contact angle; σ is the surface tension of mercury; and P is the mercury-intrusion pressure.

Mercury can enter a pore only when the applied pressure reaches the capillary-pressure threshold of the pore throat; the greater the applied pressure, the smaller the accessible pore size. Theoretically, mercury intrusion can characterize pores ranging from 7.2 nm to 750 μm. In practice, the coal can withstand only limited pressure, and information obtained for macropores and mesopores is therefore more reliable. Based on stepwise mercury-intrusion data, the theoretical permeability of each sample was calculated by integrating the Purcell capillary-bundle model. The permeability contribution of each pore-throat interval was then determined, permeability-contribution distribution curves were plotted, and dominant seepage pore throats were quantitatively identified.

(3) Nuclear magnetic resonance (NMR) experiments were performed using a MacroMR12-150H-I low-field NMR instrument [17, 18]. Before testing, the coal samples were crushed and sieved to 60–80 mesh, vacuum-dried at 105 °C for 24 h to remove free water, and then vacuum-saturated with pure water. After the T_2 spectra of the water-saturated samples were measured, the samples were centrifuged at 8,000 r/min for 1.5 h under a centrifugal pressure of 2.76 MPa to simulate the irreducible-fluid state, and the post-centrifugation T_2 spectra were measured again. Irreducible-fluid saturation (bound-fluid saturation) was calculated from the difference in total T_2 spectral area before and after centrifugation.

NMR characterization of pore structure is fundamentally based on the relaxation response of hydrogen nuclei in the pore fluid under an external magnetic field. Hydrogen nuclei resonate in the applied magnetic field; after the excitation field is removed, the nuclei release energy and return to equilibrium, a process termed relaxation. Because the coal skeleton is only weakly magnetic, the NMR signal detected under low-field conditions is derived primarily from hydrogen nuclei in the pore fluid.

The transverse relaxation rate of the pore fluid is jointly controlled by bulk relaxation, diffusion relaxation, and surface relaxation:

$$\frac{1}{T_2} = \frac{1}{T_{2B}} + \frac{1}{T_{2D}} + \frac{1}{T_{2S}}$$

where T_2 is the apparent transverse relaxation time, ms; T_{2B}, T_{2D}, and T_{2S} are the bulk-relaxation, diffusion-relaxation, and surface-relaxation times, respectively, in ms. In low-field NMR measurements of water-saturated samples, the bulk-relaxation time of the fluid, T_{2B}, can reach 2–3 s, far longer than the measured relaxation signal of the sample; because the applied magnetic field is uniform, the contribution of diffusion relaxation can also be neglected. Relaxation is therefore controlled mainly by surface relaxation arising from interactions between the fluid and pore walls, and the equation can be simplified as follows:

$$\frac{1}{T_2} = \rho_2 \frac{S}{V}$$

where ρ_2 is the transverse surface-relaxivity coefficient, nm/ms; S is the pore-surface area, nm^2; and V is the

Table 1. Basic information and associated experimental tests of coal samples collected from the study area.

Well	Stratigraphic unit	Burial depth(m)	Sample No.	R_o%	Coal rank	Coal lithotypes	Associated tests
Mei 006	J_1b	3145.42	Q1809472	0.66	Long-flame coal	Bright coal	Vitrinite reflectance, proximate analysis, ultimate analysis, maceral composition, true/apparent density, low-temperature N_2 adsorption, NMR, and isothermal adsorption
Mei 006	J_1b	3146.57	Q1809473	0.65	Long-flame coal	Bright coal	
Mei 006	J_1b	3147.06	Q1809474	0.64	Long-flame coal	Bright coal	
Mei 006	J_1b	3147.66	Q1809475	0.69	Long-flame coal	Bright coal	
Jia Tan 2	J_1b	3614.33	Q1809481	0.66	Long-flame coal	Bright coal	
Jia Tan 2	J_1b	3616.43	Q1809482	0.70	Long-flame coal	Bright coal	
Jia Tan 2	J_1b	3619.29	Q1809483	0.64	Long-flame coal	Bright coal	
Jia Tan 2	J_1b	3621.16	Q1809484	0.71	Gas coal	Bright coal	
Jia Tan 2	J_1b	3623.33	Q1809485	0.66	Long-flame coal	Semibright coal	
Jia Tan 2	J_1b	3625.23	Q1809486	0.65	Long-flame coal	Semibright coal	
Jia Tan 2	J_2x	3191.38	Q1809476	0.68	Long-flame coal	Semibright coal	
Jia Tan 2	J_2x	3192.48	Q1809477	0.78	Gas coal	Semibright coal	
Jia Tan 2	J_2x	3193.26	Q1809478	0.66	Long-flame coal	Semibright coal	
Jia Tan 2	J_2x	3194.24	Q1809479	0.71	Gas coal	Semibright coal	
Jia Tan 2	J_2x	3195.03	Q1809480	0.71	Gas coal	Semibright coal	

pore volume, nm^3. Thus, the larger the pore size, the longer the T_2 relaxation time.

The measured NMR echo signal is the superposition of relaxation signals from pores of different sizes:

$$M(t) = \sum M_i(0)e^{-t/T_{2i}}$$

A T_2 spectrum is obtained by multi-exponential inversion. A pore-shape factor F_s is then introduced to establish a quantitative relationship between relaxation time and pore radius:

$$\frac{1}{T_2} = F_s\frac{\rho_2}{r}$$

Defining the conversion coefficient $C = 2F_s\rho_2$ yields the following relationship between pore diameter and relaxation time:

$$D = CT_2$$

where F_s is the pore-geometry factor ($F_s = 3$ for spherical pores and $F_s = 2$ for cylindrical pores); r is the pore-throat radius, nm; D is the pore diameter, nm; and C is the pore-size conversion coefficient, nm/ms. Using this equation, the T_2 spectrum can be converted into a full-scale pore-size distribution.

It should be noted that when NMR T_2 is converted to an absolute pore-size distribution, the conversion coefficient C depends on accurate calibration of the coal surface relaxivity (ρ_2). Because a reliable calibration procedure for absolute pore-size alignment between high-pressure mercury intrusion and NMR is currently unavailable, this study primarily uses the T_2 relaxation time (ms) itself to evaluate pore-distribution characteristics relatively, rather than directly relying on an uncalibrated absolute pore-size distribution. Peaks at shorter relaxation times represent small pores/micropores, whereas peaks at longer relaxation times represent macropores/mesopores.

3.2.3 Evaluation of gas-storage performance

Methane isothermal adsorption experiments were conducted volumetrically at formation temperatures of 76 °C, 96 °C, and 106 °C, over a pressure range of 0–30 MPa. Dynamic porosity and permeability tests under overburden pressure were conducted at confining pressures up to 50 MPa.

4 Experimental Results and Discussion

4.1 Geological Characteristics of the Coal Reservoirs

4.1.1 Macroscopic Coal Characteristics

Core observations show that the J_1b coal seams in wells Mei 006 and Jia Tan 2 are bright coal in section, black, structurally intact, and composed of blocky fractured coal. Cleats are relatively well developed (2–4 cleats/cm), some fractures are filled, and no partings are present. The J_2x coal seam in Well Jia Tan 2 is semibright or dull coal, grayish black, blackish gray, or black, with an intact and blocky structure and a multilayered cross-section. It consists mainly of primary-structure coal, with some fractured coal. Cleats are poorly developed, fractures occur sporadically, and carbonaceous-mudstone partings are

Table 2. Results of coal petrology and quality analyses in the study area.

Well	Stratigraphic unit	Proximate analysis (%)				True/apparent density (g/cm^3)	Vitrinite (%)	Inertinite (%)	R_o(%)
		Moisture	Ash	Volatile matter	Fixed carbon				
Mei 006	J_1b	1.9	2.3	44.8	52.9	1.29/1.26	74.1	19.1	0.66
Jia Tan 2	J_1b	1.9	5.5	45.3	49.2	1.32/1.29	88.3	3.2	0.67
Jia Tan 2	J_2x	4.8	3.9	30.5	65.6	1.43/1.33	57.2	38.2	0.71

present. Overall, cleat development decreases in the order: J_1b coal in Well Mei 006 > J_1b coal in Well Jia Tan 2 > J_2x coal in Well Jia Tan 2.

4.1.2 Coal Petrological and Quality Characteristics

Proximate-analysis results (Tables 1 and 2) show that both J_1b and J_2x are ultra-low-sulfur, ultra-low-ash, and ultra-low-moisture coal seams [4]. In the J_1b interval of Well Mei 006, the mean moisture, ash, volatile matter, and fixed carbon contents are 1.9%, 2.3%, 44.8%, and 52.9%, respectively; the corresponding values for the J_1b interval of Well Jia Tan 2 are 1.9%, 5.5%, 45.3%, and 49.2%; and those for the J_2x interval of Well Jia Tan 2 are 4.8%, 3.9%, 30.5%, and 65.6%. The volatile-matter content of J_2x coal is significantly lower than that of J_1b coal, mainly because the inertinite contains abundant, nonvolatile fusinite. The fixed-carbon contents of both seams are below 70%, consistent with low-rank coal.

True/apparent-density measurements show that the true density of the coal samples ranges from 1.27 to 1.47 g/cm^3 and the apparent density from 1.24 to 1.35 g/cm^3. The true and apparent densities of J_2x coal are slightly higher than those of J_1b coal, reflecting its relatively higher degree of coalification. The mean true and apparent densities are 1.29 and 1.26 g/cm^3, respectively, for the J_1b interval of Well Mei 006; 1.32 and 1.29 g/cm^3 for the J_1b interval of Well Jia Tan 2; and 1.43 and 1.33 g/cm^3 for the J_2x interval of Well Jia Tan 2, indicating a positive relationship between burial depth and degree of coalification [10, 14].

4.1.3 Maceral Characteristics

Maceral identification shows that coal from the J_1b interval of Well Mei 006 is dominated by telocollinite (74.1%), followed by desmocollinite; the liptinite group is dominated by sporinite (2.9%), and the inertinite group by fusinite (19.2%). Coal from the J_1b interval of Well Jia Tan 2 has a vitrinite content as high as 88.3%, dominated by desmocollinite, and an inertinite content of only 3.2%. Coal from the J_2x interval of Well Jia Tan 2 has a vitrinite content of 57.2%, dominated by telocollinite, whereas the inertinite content increases markedly to 38.2% and is dominated by fusinite.

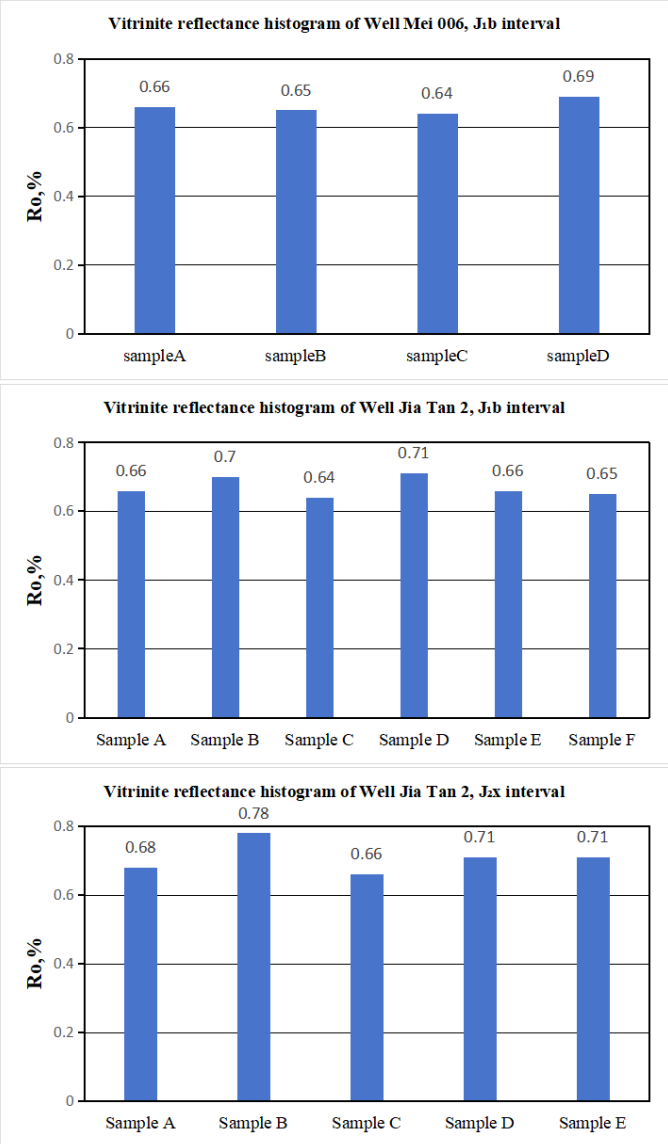

Figure 1. Distribution of vitrinite reflectance in coal from the study area.

These differences reveal distinct peat-forming environments for the two coal seams. The J_1b coal seam formed mainly through gelification,

reflecting biochemical gelification under strongly water-covered, anoxic conditions; the J_2x coal seam formed mainly through fusinization associated with decay under relatively dry and oxidizing conditions [4]. This understanding is important for interpreting pore-development characteristics in coal reservoirs at different stratigraphic levels.

Vitrinite reflectance measurements (Figure 1) show that R_o ranges from 0.55% to 0.75%, with an average of 0.67%, in the J_1b interval, and from 0.60% to 0.85%, with an average of 0.71%, in the J_2x interval. According to coal-rank classification criteria, the study-area coal is dominated by long-flame coal and lignite and is therefore typical low-rank coal. The slightly higher R_o of J_2x coal than J_1b coal indicates numerically that it approaches the medium-rank metamorphic stage.

5 Pore-space Characteristics of the Coal Reservoirs

5.1 Integrated Multi-method Characterization of Pore Structure

Pore-size classification is an essential basis for comparing and calibrating coal-reservoir pore characteristics at the microscopic scale. Numerous researchers have classified coal pore systems from different perspectives and for different purposes. The two most representative schemes are the pore-size classification proposed in 1972 by the International Union of Pure and Applied Chemistry (IUPAC)—micropores < 2 nm, mesopores 2–50 nm, and macropores > 50 nm—and the coal pore-size decimal classification proposed by the Soviet scholar Hodot (1966) (converted here to pore diameter: macropores $> 10^5$ nm, mesopores 10^2–10^5 nm, transition pores or small pores 10–10^2 nm, and micropores < 10 nm). This study follows the Hodot decimal classification widely used by Chinese researchers.

Coal-reservoir pore sizes span a broad range of 6–7 orders of magnitude, and no single method can cover the full pore-size range. This study integrates low-temperature N_2 adsorption, high-pressure mercury intrusion, and NMR to achieve multiscale, integrated characterization of coal pore structures [16–18].

(1) Low-temperature N_2 adsorption characteristics

Low-temperature N_2 adsorption experiments were conducted volumetrically to analyze the microstructural characteristics of adsorption pores, in accordance with Chinese standard GB/T 19587–2004. The experimental results were analyzed using the BET and BJH methods described above. The BET specific surface area (S_{BET}) ranges from 0.124 to 33.1 m^2/g, the BJH total pore volume (V_{BJH}) from 0.0008 to 0.0236 cm^3/g, and the mean pore diameter from 3.64 to 51.84 nm. In the J_1b interval of Well Mei 006, S_{BET} ranges from 0.124 to 0.52 m^2/g (mean 0.334 m^2/g), V_{BJH} from 0.0015 to 0.0025 cm^3/g (mean 0.0019 cm^3/g), and mean pore diameter from 11.75 to 51.84 nm (mean 30.72 nm). In the J_1b interval of Well Jia Tan 2, S_{BET} ranges from 0.337 to 0.423 m^2/g (mean 0.385 m^2/g), V_{BJH} from 0.0009 to 0.001 cm^3/g (mean 0.0009 cm^3/g), and mean pore diameter from 8.52 to 10.49 nm (mean 9.6 nm). In the J_2x interval of Well Jia Tan 2, S_{BET} increases markedly to 5.22–33.12 m^2/g (mean 18.35 m^2/g), V_{BJH} is 0.0072–0.0236 cm^3/g (mean 0.0166 cm^3/g), and mean pore diameter is 3.64–5.53 nm (mean 4.64 nm).

These data show that the specific surface area and pore volume of the J_2x coal seam are both significantly greater than those of the J_1b coal seam, whereas its mean pore diameter is smaller, indicating that micropores are more developed in J_2x coal and provide a larger surface area for methane adsorption.

Based on the shapes of the low-temperature N_2 adsorption and desorption curves, the coal samples from the study area can be divided into three types (Figure 2).

Type A: The adsorption branch rises steadily and the desorption branch exhibits a distinct hysteresis loop, indicating pores dominated by cylindrical or slit-shaped geometries. The mean pore diameter is 4–8 nm, and S_{BET} and V_{BJH} are relatively large. This pore structure contains both micropores favorable for CBM adsorption and mesopores with relatively good gas conductivity, facilitating CBM adsorption, desorption, and diffusion. Most J_2x coal samples from Well Jia Tan 2 are Type A.

Type B: The curve rises slowly in the early stage and sharply in the late stage, with a weak hysteresis loop, representing a typical bimodal pore structure in which both small pores and micropores are abundant. Pore-volume peaks occur at 4 and 30 nm, the mean pore diameter exceeds 10 nm, and S_{BET} and V_{BJH} are relatively small. The pores are mainly gas-conductive parallel-plate and wedge-shaped pores. Most J_1b coal samples from Well Jia Tan 2 are Type B.

Type C: The curve is similar to that of Type B, but

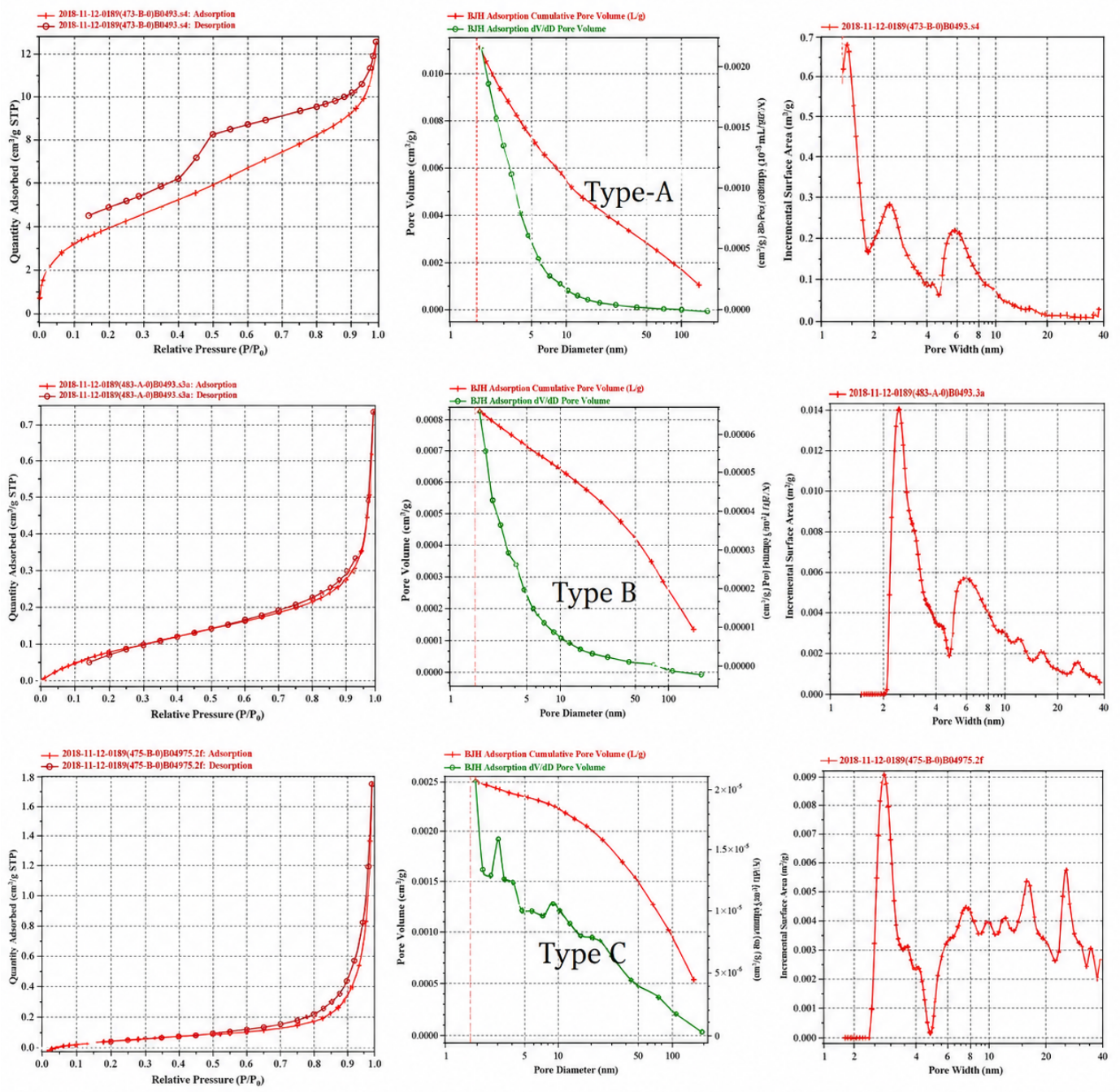

Figure 2. Typical low-temperature N_2 adsorption–desorption curve types of coal samples from the study area.

Table 3. Results of mercury-intrusion analyses of coal from the study area.

Well	Stratigraphic unit	Porosity (%)	Permeability (mD)	Maximum pore-throat radius (μ m)	Median radius (μm)	Mercury-withdrawal efficiency (%)
Mei 006	J_1b	3.8	5.61	22.536	0.0101	78.6
Jia Tan 2	J_1b	4.5	3.88	16.651	0.0161	70.8
Jia Tan 2	J_2x	9.4	19.64	22.986	0.1346	53.2

remains nearly flat at $P/P_0 < 0.9$ and then rises sharply. The mean pore diameter is relatively large (approximately 38 nm), whereas S_{BET} and micropore volume are extremely small. Micropores are poorly developed, connectivity is low, and the pore structure is dominated by parallel-plate and wedge-shaped

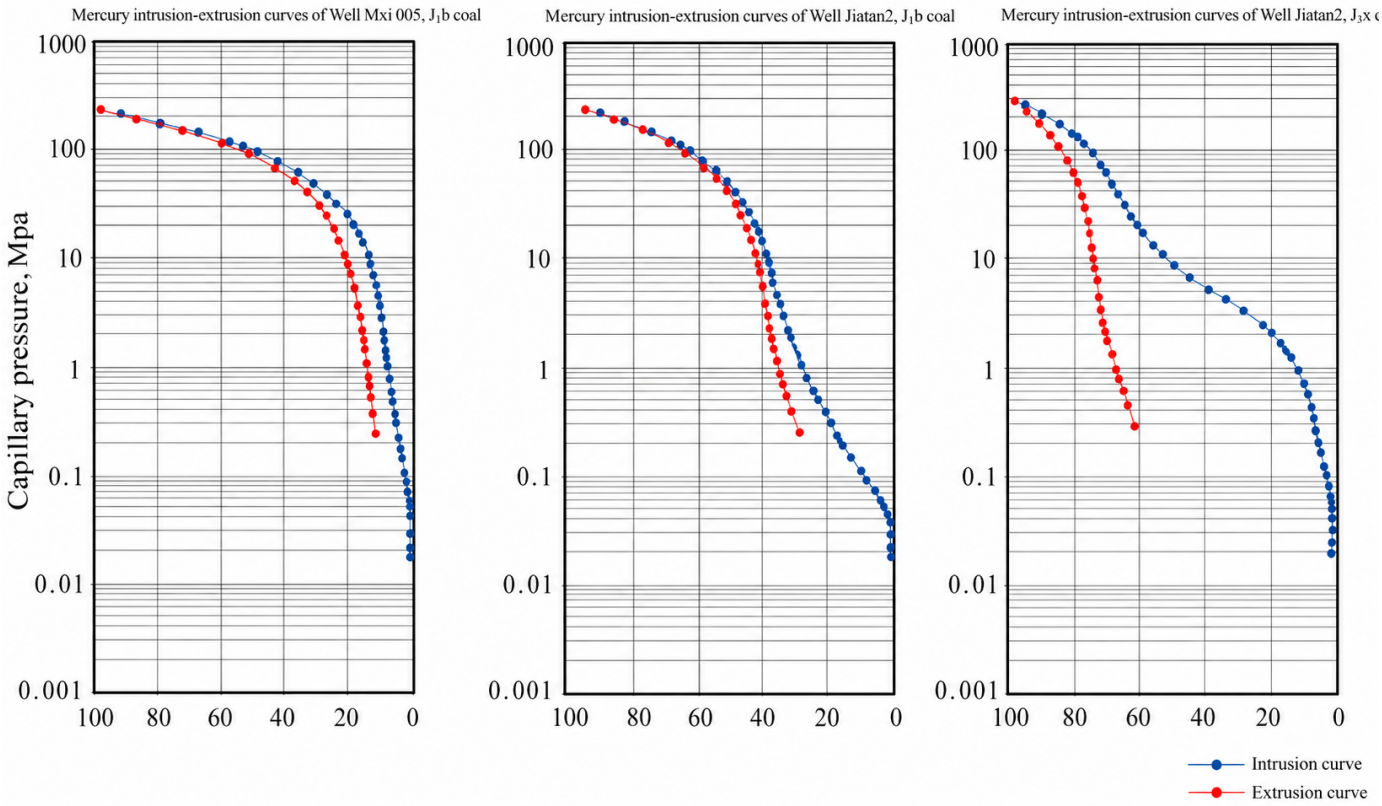

Figure 3. Mercury-intrusion capillary-pressure curves of representative coal samples from the study area (left: J_1b interval of Well Mei 006; middle: J_1b interval of Well Jia Tan 2; right: J_2x interval of Well Jia Tan 2).

pores closed at one end. Most J_1b coal samples from Well Mei 006 are Type C.

(2) High-pressure mercury-intrusion characteristics

Mercury-intrusion results (Table 3) show that the J_1b coal in Well Mei 006 has a maximum pore-throat radius of 22.536 μm, a median radius of 0.0101 μm, a mean porosity of 3.8%, and a mean permeability of 5.61 mD. The J_1b coal in Well Jia Tan 2 has a maximum pore-throat radius of 16.651 μm, a median radius of 0.0161 μm, a mean porosity of 4.5%, and a mean permeability of 3.88 mD. The J_2x coal in Well Jia Tan 2 has a maximum pore-throat radius of 22.986 μm, a median radius of 0.1346 μm, a mean porosity of 9.4%, and a mean permeability of 19.64 mD.

The median radius of the J_2x coal seam (0.1346 μm) is one order of magnitude greater than that of the J_1b coal seam (0.0101–0.0161 μm), and its proportions of macropores and mesopores are higher. Although the median radius of J_2x coal is significantly larger than that of J_1b coal, its mercury-withdrawal efficiency (mean 53.2%) is markedly lower than that of the J_1b interval (70.8%–78.6%). This apparent contradiction is mainly attributable to the widespread development of ink-bottle pores and heterogeneity within the pore network of J_2x coal. Although the large pore throats of J_2x coal provide favorable fluid-entry pathways, narrow throats cause a pronounced mercury-entrapment effect during mercury withdrawal, leaving substantial mercury trapped in the larger internal pore bodies. Therefore, high mercury-withdrawal efficiency alone cannot be regarded as definitive evidence of good connectivity. A comprehensive assessment is required: despite its low mercury-withdrawal efficiency, J_2x coal has a larger absolute pore-throat scale, which is the decisive factor ensuring its high permeability and dominant seepage capacity. The mean mercury-withdrawal efficiencies are 78.6% for the J_1b interval of Well Mei 006, 70.8% for the J_1b interval of Well Jia Tan 2, and 53.2% for the J_2x interval of Well Jia Tan 2. Mercury-withdrawal efficiency characterizes pore morphology, whereas pore-throat scale is more critical in controlling seepage capacity: the larger pore throats of J_2x coal effectively reduce gas-flow resistance (Figure 3).

(3) Nuclear magnetic resonance (NMR) characteristics

NMR T_2 spectral analysis quantitatively characterizes pore-size distributions [17, 18]. In the J_1b interval of Well Mei 006, micropores, small pores, mesopores, and macropores account on average for 49.2%, 14.1%, 7.4%,

and 29.4%, respectively (with micropores reaching 65.3% in some samples); the mean NMR porosity is 3.806%, and bound-fluid saturation is as high as 94.55%. In the J_1b interval of Well Jia Tan 2, the corresponding mean proportions are 72.3%, 19.1%, 4.0%, and 4.6%; mean NMR porosity is 4.11%, and bound-fluid saturation is as high as 97.22%. In the J_2x interval of Well Jia Tan 2, the corresponding mean proportions are 12.95%, 33.65%, 24.4%, and 29.0% (with micropores reaching 50.4% in some samples); mean NMR porosity is 8.757%, and bound-fluid saturation is 66.61%.

The NMR results clearly reveal the fundamental difference between the pore structures of the two coal seams. Micropores overwhelmingly dominate the J_1b coal seam (49%–72%), mesopores and macropores are limited, and bound-fluid saturation is extremely high (94%–97%), indicating poor pore connectivity and little movable fluid. In the J_2x coal seam, pore types are more evenly distributed, with small pores, mesopores, and macropores each accounting for substantial proportions; bound-fluid saturation is relatively low (66.61%), indicating better pore connectivity and a higher proportion of movable fluid (Figure 4).

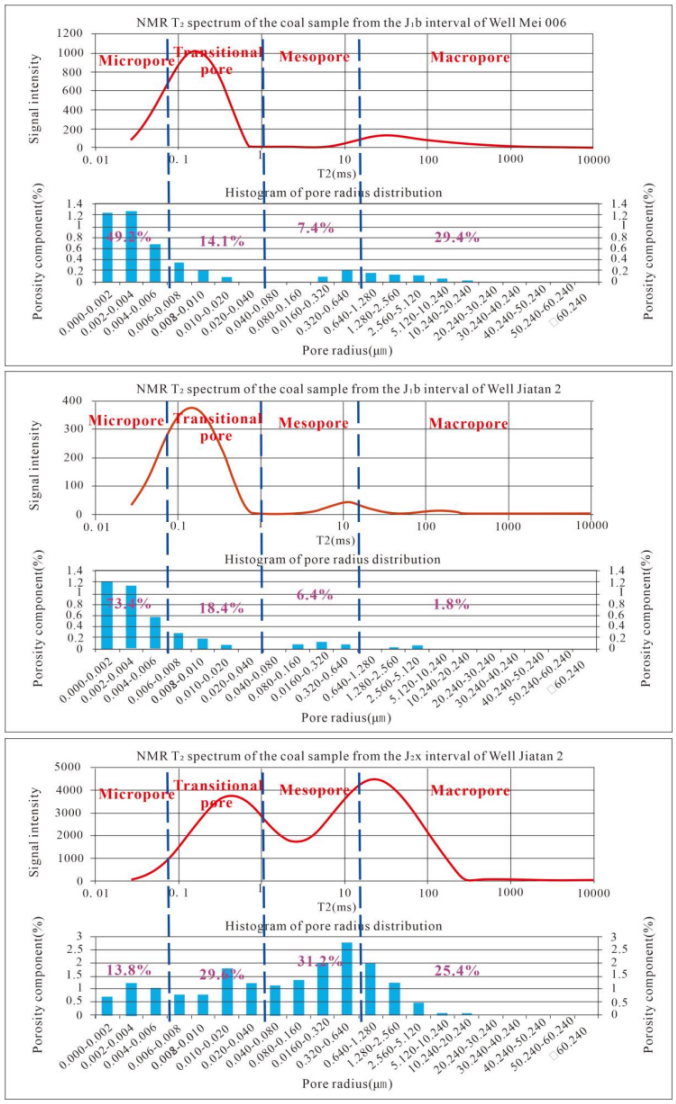

Figure 4. NMR T_2 spectra of representative coal samples from the study area (top: J_1b interval of Well Mei 006; middle: J_1b interval of Well Jia Tan 2; bottom: J_2x interval of Well Jia Tan 2).

5.1.1 *Principal Controls on Pore-space Development*

The integrated multi-method characterization results indicate that pore-space development in the low-rank coal reservoirs of the study area is controlled by the following factors:

(1) Maceral composition: J_1b coal, with a high vitrinite content (74%–88%), formed mainly through gelification and has a relatively homogeneous maceral composition, with pores dominated by small pores and micropores. J_2x coal, with a high inertinite content (38.2%), formed mainly through fusinization; fusinite commonly occurs in reticulate, banded, and fragmental forms, with well-developed primary tissue pores and cell-lumen pores and consequently more diverse pore types.

(2) Degree of coalification: The R_o of J_2x coal (0.71%) is slightly higher than that of J_1b coal (0.67%), indicating a somewhat higher degree of coalification. As coalification increases, compaction and thermal evolution modify the pore structure and increase the proportion of micropores; however, the high inertinite content of J_2x coal preserves more mesopores and macropores [19].

(3) Depositional environment: J_1b coal formed in a strongly water-covered, anoxic environment. Intense gelification homogenized the original plant tissues, and the pores are dominated by micropores formed during gelification. J_2x coal formed under relatively dry and oxidizing conditions; fusinization preserved more plant-tissue pores and cell-lumen pores, resulting in a richer variety of pore types [20].

(4) Burial depth: The J_1b coal in Well Mei 006 is buried at approximately 3,145 m, whereas that in Well Jia Tan 2 is buried at approximately 3,615 m. The porosity and pore-throat scale of the J_1b coal in Well Mei 006 are both greater than those in Well Jia Tan 2, indicating that shallower burial and weaker compaction favor the preservation of large pores [6, 14].

Table 4. Commonly used adsorption models and their basic assumptions.

Model	Common equation	Basic assumptions
Langmuir adsorption model	$V = V_L \frac{P}{P_L + P}$	1. Adsorption is in dynamic equilibrium. 2. The adsorbent surface is homogeneous. 3. No interactions occur among adsorbed gas molecules. 4. Adsorption equilibrium on the solid surface forms only a monolayer.
Extended Langmuir adsorption model	$V = \frac{V_L K_b P}{1 + K_b P + n\sqrt{K_b P}}$	Same as above.
BET multilayer adsorption model	$\frac{P}{V(P_0 - P)} = \frac{1}{V_m C} + \frac{C-1}{V_m C}\left(\frac{P}{P_0}\right)$	1. Adsorption is in dynamic equilibrium. 2. The adsorbent surface is homogeneous. 3. No interactions occur among adsorbed gas molecules. 4. Van der Waals forces among adsorbed molecules produce multilayer adsorption. 5. The heat of adsorption of the first layer differs from that of subsequent layers.
Dubinin–Radushkevich (D–R) equation	$V = V_0 \exp\left[-\left(\frac{RT}{\beta E}\ln\frac{P_0}{P}\right)^2\right]$	1. The adsorbate follows the micropore volume-filling mechanism. 2. The filling layers within pores are continuous.
Dubinin–Astakhov (D–A) equation	$V = V_0 \exp\left[-\left(\frac{RT}{\beta E}\ln\frac{P_0}{P}\right)^n\right]$	Same as above.

Note: V, adsorption capacity (cm^3/g); P, gas pressure (MPa); V_L, Langmuir volume (cm^3/g); P_L, Langmuir pressure (MPa); P_0, saturated vapor pressure (MPa); K_b, association constant; n, heterogeneity exponent; V_m, monolayer adsorption capacity (cm^3/g); V_0, limiting adsorption capacity (cm^3/g); β, affinity coefficient; E, characteristic adsorption energy (kJ/mol); R, universal gas constant; T, temperature (K).

5.1.2 Integrated Evaluation of Reservoir Properties

According to the integrated mercury-intrusion and overburden-pressure porosity–permeability results, the J_2x coal seam has a mean porosity of 9.4% and a permeability of 19.64 mD (mercury intrusion), indicating good reservoir properties; the J_1b coal seam has a mean porosity of 3.8%–4.5% and a permeability of 3.88–5.61 mD, indicating poor reservoir properties. Under an overburden pressure of 50 MPa, the porosities of both J_1b and J_2x coal tend to stabilize. However, when pressure is increased beyond 50 MPa, the permeability of J_2x coal continues to decrease at a relatively high rate, indicating greater pressure sensitivity of its pore structure.

Overall analysis of individual factors indicates that J_2x coal has slightly better pore space than J_1b coal. Regionally, the reservoir properties of J_1b coal in the Baijiahai area are generally comparable to those in the Dinan area, although the pore space and pore-throat connectivity of J_1b coal are slightly better in the Dinan area, where the proportions of macropores and mesopores are also slightly higher [11, 14].

5.2 Gas Storage Mechanisms in the Coal Reservoirs

5.2.1 Adsorbed-gas storage mechanism

(1) Isothermal adsorption characteristics

The isothermal adsorption experiments show that methane adsorption is jointly controlled by temperature and pressure. At a given pressure, a lower temperature results in a greater adsorbed-gas capacity because gas adsorption is an exothermic physical process and is generally promoted by cooling. At a given temperature, the adsorbed-gas capacity increases markedly with pressure below 15 MPa and gradually approaches saturation at pressures approaching 30 MPa [4]. All isothermal adsorption data reported in this study were consistently normalized to a dry ash-free (DAF) basis.

The critical desorption pressure was back-calculated using the classical Langmuir equation and measured parameters. The Langmuir volume and Langmuir pressure of each coal sample were first fitted from the isothermal adsorption curves. These parameters were then combined with formation-pressure conditions in the study area and measured/literature-derived in-situ original gas contents to calculate the pressure threshold at which gas begins to desorb extensively from the coal matrix. The results show that the critical desorption pressure of J_2x coal is 3.7–4.7 MPa and that the maximum adsorption capacity reaches 17 m^3/t under high-temperature (formation-temperature) conditions. For J_1b coal, the

critical desorption pressure is 4.5–6.8 MPa and the maximum adsorption capacity is 12.8 m^3/t [3, 11] (Figure 5).

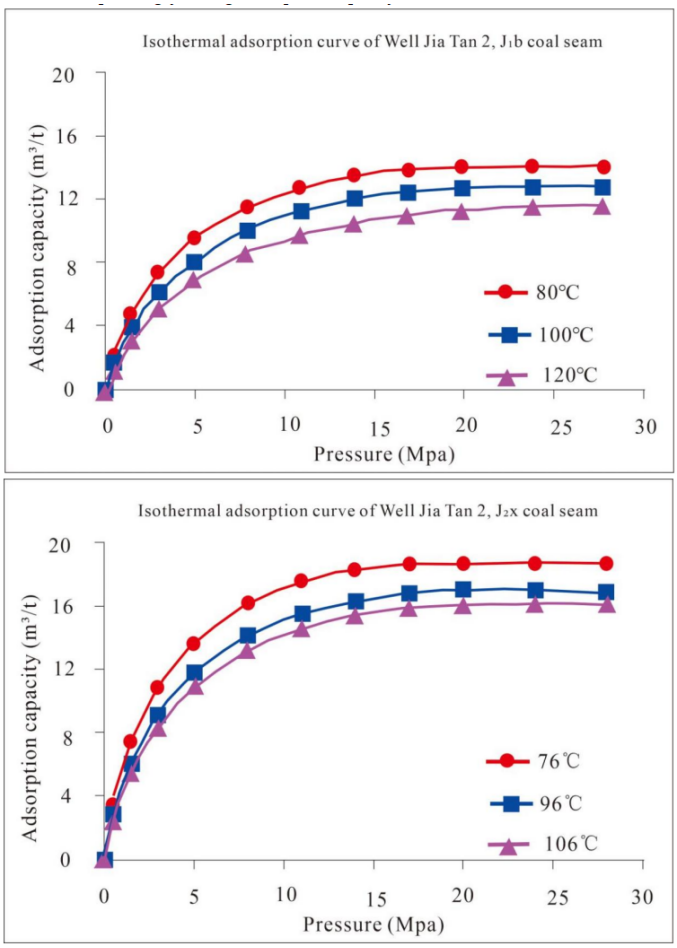

Figure 5. Methane isothermal adsorption curves of coal samples from the study area.

In terms of coal composition, fixed-carbon content is positively correlated with adsorbed-gas capacity: the higher the fixed-carbon content, the greater the Langmuir volume, the lower the Langmuir pressure, and the greater the adsorption capacity. The J_2x interval of Well Jia Tan 2 has a relatively high fixed-carbon content (65.6%) and correspondingly strong adsorption capacity.

(2) Adsorption theory applicable to low-rank coal

Based on analysis of adsorption within individual pores, this study proposes an adsorption-theory model applicable to low-rank coal [8]. The theoretical basis of the different adsorption models and their respective assumptions are summarized in Table 4. The classical Langmuir monolayer adsorption theory assumes a uniform energy state on the solid surface, one molecule per adsorption site, and no interactions among adsorbed molecules. These assumptions deviate from the actual complex pore structure of coal, and a new adsorption model is therefore developed in this study as described below.

The low-temperature N_2 isothermal adsorption process can be divided into four stages. At extremely low pressure, adsorption occurs mainly in micropores, which are rapidly filled. As pressure increases, molecules begin to adsorb on pore surfaces, predominantly as a monolayer. Multilayer adsorption occurs at intermediate pressure, and even large pores become filled at high pressure. For an individual pore, the smaller the pore diameter, the faster the entire adsorption process is completed: micropores > transition pores > mesopores > macropores.

Based on this understanding, adsorption behavior in pores of different sizes can be summarized as follows (Figure 6). At a given reservoir temperature and pressure, micropores rapidly reach a filled state (which can also be regarded as monolayer adsorption saturation), transition pores approach monolayer adsorption saturation, and mesopores and macropores remain in an unsaturated monolayer adsorption state. The J_1b coal seam has a high micropore proportion (49%–72%), reaches adsorption saturation rapidly, and has a large adsorption capacity, showing a tendency toward adsorption saturation at reservoir pressure. The J_2x coal seam has a low micropore proportion (approximately 13%), reaches saturation slowly, and its adsorption capacity is strongly influenced by adsorption in transition pores and mesopores; no clear saturation trend is observed at reservoir pressure [9, 20].

This theory better explains the adsorption behavior of low-rank coal and also explains why J_1b coal, despite its lower porosity and permeability, has a higher gas content: well-developed micropores provide abundant adsorption sites.

5.2.2 Free-gas storage mechanism

(1) Microscopic controls on free-gas storage

Coal-reservoir pores can be divided into three categories: matrix adsorption pores (nanoscale, including micropores and transition pores), matrix pores (microscale, including mesopores and macropores), and fracture seepage pores (millimeter scale). Gas occurrence differs among these pore types. Gas in micropores occurs mainly in the adsorbed state, leaving very little effective space for free gas; adsorbed and free gas coexist in transition pores; mesopores and macropores are the principal

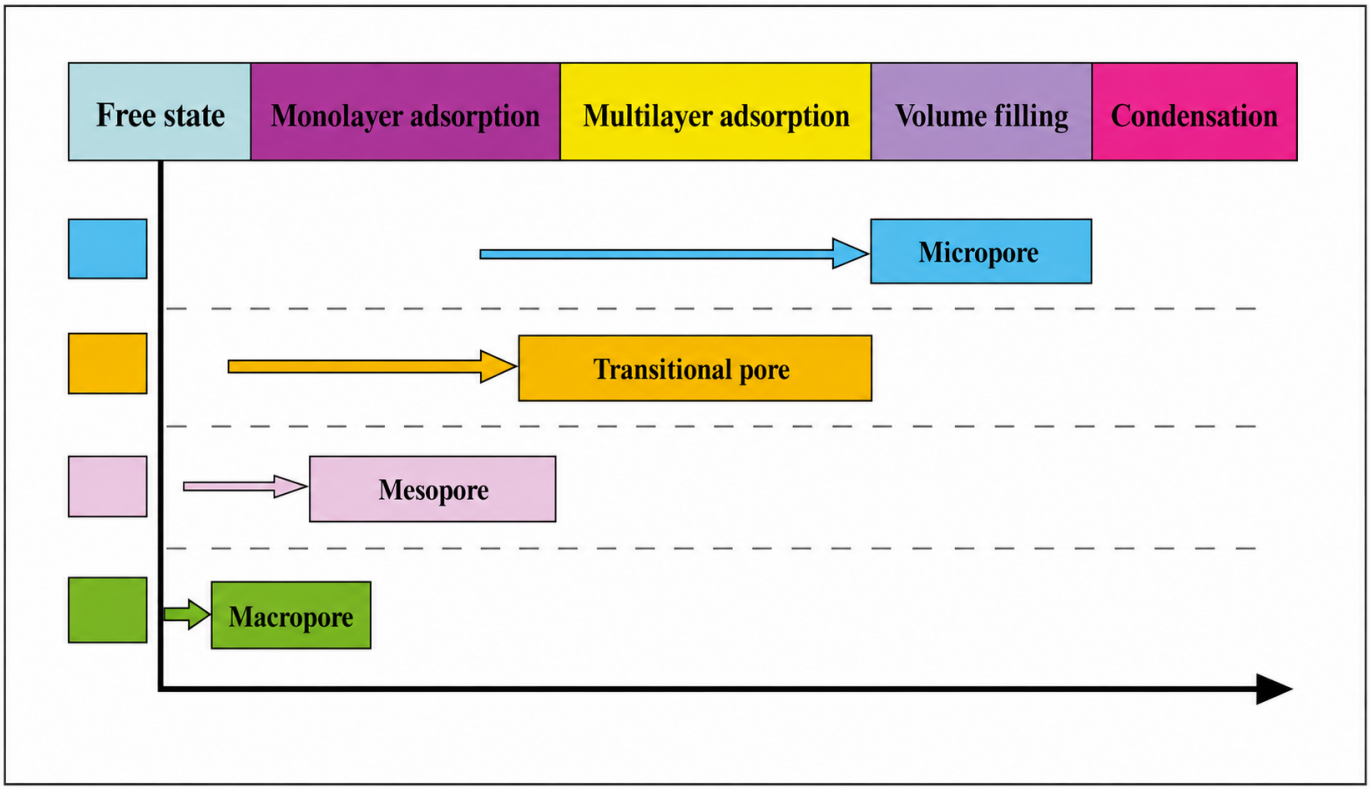

Figure 6. Schematic diagram of adsorption processes in pores of different sizes.

spaces for free-gas occurrence; and fracture seepage pores contain mainly liquid water, together with small amounts of free and dissolved gas.

The relatively well-developed mesopores and macropores in low-rank coal provide favorable storage sites for free gas. However, under the present formation-temperature and pressure conditions, CBM still occurs predominantly in the adsorbed state within micropores and transition pores, and the proportion of free gas remains low. Estimates indicate that free gas accounts for only 2.89%–5.14% of total gas content in the principal Xishanyao coal seams along the southeastern margin of the Junggar Basin [3]. Although the overall proportion is low, compared with medium- and high-rank coal, the J_2x low-rank coal reservoir in the study area has higher pore volume and specific surface area, giving it relatively greater potential for secondary free-gas storage.

Competition from water for pore space cannot be ignored. Water can occupy adsorption sites on the coal surface and reduce the number of effective sites available for methane adsorption. This competition involves not only water and adsorbed gas but also free gas [20]. In matrix adsorption pores, free liquid water cannot enter the small pores; water is mainly bound to coal through physicochemical interactions and is regarded as inherent moisture. In matrix pores, water occurs as weakly bound water and is the principal competitor for effective free-gas storage space. Fracture seepage pores are dominated by liquid water.

(2) Macroscopic controls on free-gas storage

At the macroscopic scale, in-situ free-gas storage is controlled by structural-geological, hydrodynamic, and lithological conditions. During the primary thermogenic-gas stage of low-rank coal, gas migrates outward and is extensively lost in the absence of effective trapping boundaries, particularly during tectonic uplift and under strong hydrodynamic conditions. As temperature and pressure decrease, the adsorption capacity of the coal reservoir declines, adsorbed gas is converted to free gas, and the gas migrates further toward zones of lower concentration [3, 4].

Early biogenic-gas generation in the low-rank coal of the Junggar Basin was limited, but active formation water transported methanogens into the coal seams, where degradation generated abundant secondary biogenic gas that replenished the CBM reservoirs. Hydrogeological conditions profoundly influence the accumulation of low-rank CBM. Tectonic movements also exert a marked influence on CBM reservoirs, and the dynamic exchange between adsorbed and free

gas through geological time is controlled mainly by tectonic activity [5, 6].

Gas-content distribution in the study area shows that the gas content of the J_1b coal seam is generally higher than that of the J_2x coal seam. In the Baijiahai area, the highest gas contents in the J_1b coal seam occur near wells Cai 35, Jia Tan 2, and Dinan 081, where values exceed 16 m^3/t. Gas content is positively correlated with carbon content and is generally higher in areas with higher carbon content. It is also closely related to burial depth, showing an overall increase with increasing coal-seam depth. Gas content is related to coal-seam thickness as well and generally increases with seam thickness. Structurally, gas content is higher within nose structures, lower in gently deformed areas, and readily dissipated near faults [3, 11, 14].

6 Conclusions

(1) In the Baijiahai–Dinan area of the Junggar Basin, J_1b coal is bright coal with an intact structure, blocky fractured texture, relatively well-developed cleats, a vitrinite content of 74.1%–88.3%, and an average R_o of 0.67%. J_2x coal ranges from semibright to dull coal, consists mainly of primary-structure coal, has poorly developed cleats, a vitrinite content of 57.2%, and an average R_o of 0.71%. Both seams are ultra-low-sulfur, ultra-low-ash, and ultra-low-moisture coals in the long-flame coal–lignite range. J_1b coal formed mainly through gelification, whereas J_2x coal formed mainly through fusinization.

(2) The J_2x coal seam contains diverse pore types, including plant-tissue pores and secondary pores, and has better physical properties, pore size, pore volume, and specific surface area than the J_1b coal seam, with a mean porosity of 9.4% and permeability of 19.64 mD. The pore space of the J_1b coal seam is dominated by small pores and micropores, with a mean porosity of 3.8%–4.5% and permeability of 3.88–5.61 mD. The low-temperature N_2 adsorption curves can be divided into Type A (cylindrical/slit-shaped pores), Type B (parallel-plate/wedge-shaped pores), and Type C (pores closed at one end), corresponding to different pore morphologies and connectivity characteristics.

(3) Based on analysis of adsorption within individual pores, an adsorption theory applicable to low-rank coal is proposed: micropores rapidly reach a filled state at extremely low pressure, transition pores approach monolayer adsorption saturation, and mesopores and macropores remain in an unsaturated monolayer adsorption state. The critical desorption pressure of J_2x coal is 3.7–4.7 MPa, and its maximum adsorption capacity at high temperature reaches 17 m^3/t; the critical desorption pressure of J_1b coal is 4.5–6.8 MPa, and its maximum adsorption capacity is 12.8 m^3/t.

(4) Free-gas storage is jointly controlled at microscopic and macroscopic scales. Microscopically, mesopores and macropores are the principal spaces for free-gas occurrence; macroscopically, structural, hydrodynamic, and lithological conditions control free-gas dissipation. In terms of storage performance, the favorable porosity and permeability of J_2x coal promote free-gas storage and fluid seepage; whereas the extremely well-developed micropores of J_1b coal result in higher maximum adsorption capacity and gas content. The two seams therefore have different advantages in their storage mechanisms, and both have substantial exploration and development potential.

(5) Integrated multi-method characterization demonstrates that low-rank coal reservoirs have strongly heterogeneous pore structures that cannot be fully characterized by any single method. The integrated use of low-temperature N_2 adsorption and high-pressure mercury intrusion with NMR enables systematic characterization of pore structures from nanometer to millimeter scales and provides an effective methodological framework for evaluating low-rank coal reservoirs.

Data Availability Statement

Data will be made available on request.

Funding

This work was supported without any funding.

Conflicts of Interest

Yuqing Chen and Yi Wang are affiliated with the Xinjiang Yaxin Coalbed Methane Resource Technology Research Co., Ltd., Urumqi 830011, China. The authors declare that this affiliation had no influence on the study design, data collection, analysis, interpretation, or the decision to publish, and that no other competing interests exist.

AI Use Statement

The author declares that no generative AI was used in the preparation of this manuscript.

Ethical Approval and Consent to Participate

Not applicable.

References

[1] Changbo, C., Hulin, Y., Fubing, L., Chenglin, L., Jie, Z., & Yuxi, L. (2008). Exploration and development prospects of coal bed methane (CBM) resources in China. *China Mining Magazine, 17*(5), 1-4. http://www.chinaminingmagazine.com/en/article/id/314d5457-ffc4-4132-884d-542c2fae9e97

[2] Wang, Y. T., Xie, S., Liu, Q. Y., He, L. J., & Meng, Q. H. (2002). Analysis of low-rank coalbed methane resources and exploration potential in Junggar Basin. *Journal of Xinjiang Petroleum Institute, 2002*(3), 5-7+12. https://caod.oriprobe.com/articles/17465918/The_Analysis_of_the_Resources_and_Exploration_Pote.htm

[3] Luo, B., Wang, H., Sun, B., Ouyang, Z., Yang, M., Wang, Y., & Zhou, X. (2024). Gas Content and Geological Control of Deep Jurassic Coalbed Methane in Baijiahai Uplift, Junggar Basin. *Processes, 12*(12), 2671. [CrossRef]

[4] Yuan, Y. U. A. N., Shan, Y., Tang, Y., & Cao, D. (2020). Coalbed methane enrichment regularity and major control factors in the Xishanyao Formation in the western part of the southern Junggar Basin. *Acta Geologica Sinica-English Edition, 94*(2), 485-500. [CrossRef]

[5] Bustin, R. M., & Clarkson, C. R. (1998). Geological controls on coalbed methane reservoir capacity and gas content. *International Journal of Coal Geology, 38*(1-2), 3-26. [CrossRef]

[6] Moore, T. A. (2012). Coalbed methane: A review. *International Journal of Coal Geology, 101*, 36-81. [CrossRef]

[7] Clarkson, C. R., & Bustin, R. M. (2011). Coalbed methane: current field-based evaluation methods. *SPE Reservoir Evaluation & Engineering, 14*(01), 60-75. [CrossRef]

[8] Cao, D. Y., Yao, Z., & Li, J. (2014). Evaluation status and development trend of unconventional gas in coal measure. *Coal Sci. Technol, 42*(1), 89-92. https://www.mtkxjs.com.cn/en/article/id/ae5aef03-cda4-4b01-841d-9d78dd5ee301

[9] Clarkson, C. R., & Bustin, R. M. (1999). The effect of pore structure and gas pressure upon the transport properties of coal: a laboratory and modeling study. 2. Adsorption rate modeling. *Fuel, 78*(11), 1345-1362. [CrossRef]

[10] Fu, H., Tang, D., Xu, T., Xu, H., Tao, S., Li, S., ... & Wang, L. (2017). Characteristics of pore structure and fractal dimension of low-rank coal: A case study of Lower Jurassic Xishanyao coal in the southern Junggar Basin, NW China. *Fuel, 193*, 254-264. [CrossRef]

[11] Fu, H., Tang, D., Xu, H., Xu, T., Chen, B., Hu, P., ... & He, G. (2016). Geological characteristics and CBM exploration potential evaluation: A case study in the middle of the southern Junggar Basin, NW China. *Journal of Natural Gas Science and Engineering, 30*, 557-570. [CrossRef]

[12] Carroll, A. R., Graham, S. A., & Smith, M. E. (2010). Walled sedimentary basins of China. *Basin Research, 22*(1), 17-32. [CrossRef]

[13] Li, X., Chen, G., Wu, C., Li, J., Haproff, P. J., Geng, M., ... & Yang, D. (2023). Tectono-stratigraphic framework and evolution of east Junggar Basin, central asia. *Tectonophysics, 851*, 229758. [CrossRef]

[14] Zhang, B., Tao, S., Sun, B., Tang, S., Chen, S., Wen, Y., & Ye, J. (2024). Genesis and accumulation mechanism of external gas in deep coal seams of the Baijiahai Uplift, Junggar Basin, China. *International Journal of Coal Geology, 286*, 104506. [CrossRef]

[15] Clarkson, C. R., & Bustin, R. M. (1999). The effect of pore structure and gas pressure upon the transport properties of coal: a laboratory and modeling study. 1. Isotherms and pore volume distributions. *Fuel, 78*(11), 1333-1344. [CrossRef]

[16] Tao, S., Chen, S., Tang, D., Zhao, X., Xu, H., & Li, S. (2018). Material composition, pore structure and adsorption capacity of low-rank coals around the first coalification jump: A case of eastern Junggar Basin, China. *Fuel, 211*, 804-815. [CrossRef]

[17] Yao, Y., Liu, D., Cai, Y., & Li, J. (2010). Advanced characterization of pores and fractures in coals by nuclear magnetic resonance and X-ray computed tomography. *Science China Earth Sciences, 53*(6), 854-862. [CrossRef]

[18] Yao, Y., & Liu, D. (2012). Comparison of low-field NMR and mercury intrusion porosimetry in characterizing pore size distributions of coals. *Fuel, 95*, 152-158. [CrossRef]

[19] Li, Y., Zhang, C., Tang, D., Gan, Q., Niu, X., Wang, K., & Shen, R. (2017). Coal pore size distributions controlled by the coalification process: An experimental study of coals from the Junggar, Ordos and Qinshui basins in China. *Fuel, 206*, 352-363. [CrossRef]

[20] Cai, Y., Liu, D., Pan, Z., Yao, Y., Li, J., & Qiu, Y. (2013). Pore structure and its impact on CH4 adsorption capacity and flow capability of bituminous and subbituminous coals from Northeast China. *Fuel, 103*, 258-268. [CrossRef]